Original Research Article

An Enhanced Micro-Spring Constitutive Model of Metal Rubber

ABSTRACT

Metal rubber (MR), as a new hysteresis non-linear elastic material with unique properties, has been extensively used in recent years, especially in aviation, aerospace and harsh conditions while the relevant theoretical research is still in the initial stage. In this paper, an effective constitutive model is established to describe the nonlinear mechanical behaviour and complex micro-contact frictional phenomena of MR. An adaptive deformation micro-spring element with random spatial distribution is adopted in this model based on the irregular overlapping, interlacing and force-deformation characteristics of metal wire material. The laws of load deformation and the frictional contact of the MR wires are considered in the model. Starting from the micro-spring force, an enhanced constitutive model including macroscopic parameters, such as shape factor, relative density, filament diameter and spiral coil diameter of MR, and microstructural parameters, such as spatial orientation angle of wires, the ratio of the micro-spring states and friction coefficient is developed for the first time. The feasibility of the enhanced constitutive model is verified by comparing the analytical results computed by the theoretical model, the numerical results of dynamic simulation based on the virtual prototype model, and the experimental results of MR under unidirectional tests. Finally, the accuracy of the model is conducted through being compared with the porous material model and the curved cantilever beam model. The results demonstrated that the characteristics of MR, especially its nonlinear stiffness, are well modelled in the enhanced micro-spring model.

Keywords: metal rubber; constitutive model; micro-spring; nonlinear stiffness; hysteresis damping

1. INTRODUCTION

Metal rubber (MR) is a high-performance damping material mainly used in the extremely harsh environment [1,2] shown in Fig.1. Because its deformation characteristic is similar to that of elastic rubber, it is also called tangled wire materials (TMW) [3] or elastic porous metal rubber (EPMR) [4]. The excellent mechanical properties of MR depend on the unique structure of entangled wires within the material, which is directly related to its very complex manufacturing process. Modelling of MR has become fundamentally important for the analysis and design of its mechanical properties.

Mathematical models based on curve fitting of experimental data and intrinsic physical structure analysis are generally adopted to represent MR [5-8]. Curve fitting models normally are phenomenological models and cannot reveal the real physical mechanisms of MR. The constitutive model, however, can describe and explain its mechanical properties. In the innovation of classical models, Chen [9] proposed a small curved beam model to reflect the effects of raw material, filament diameter, density, helical diameter and relative density of

MR on the stress-strain relationship. Li [10] regarded MR as porous solids and established its porous material constitutive model. Cao [11] employed a single turn spiral coil structure based on a variable length cantilevered beam, and derived the constitutive model of MR. Also spirals are employed as beams, Hou [12] introduced an intrinsic structure based on the geometric relationship between spiral coils and simply supported beams. The established models still have difficulties to represent the micro structure of MR and to describe its macroscopic behaviour.

Evidently, from the constructed modelling equations, physically meaningful parameters can give information about the real properties of a model. Rodney [13] studied the Poisson function made of copper, shape memory alloy metal (Ni-Ti) and polyamide by means of a discrete element simulation, and pointed out that MR could exhibit a unique strain-dependent Poisson function. Ma [14] further investigated the tangent modulus and the loss factor of SMA-MR under different constraints. Pre-compression and excitation amplitude exhibit a noticeable effect on the mechanical behaviour reported by Chandrasekhar [15], and cross-section distortion and specific geometric coefficient associated with the cyclic vibration reliability of the annular MR was reasonably proposed from Yang [16]. An optimal design guideline associated with structural parameters was offered by their research work. Therefore, constructing a proper and effective constitutive model has both theoretical and practical meanings for the design, manufacturing, and application of MR.

(a) A cylindrical metal rubber specimen (b) The constructed model of the specimen.

Fig. 1. A metal rubber (MR) specimen and its constructed model

Based on the characteristics of the micro-contact of MR wires and the macroscopic deformation of MR, an adaptive deformation micro-spring model with random spatial distribution is proposed in this paper. The model utilizes the distribution of the micro-spring orientation angle to characterize MR. By analyzing the deformation along the axial and radial directions when subjected to load, the analytical expression of stress-strain relationship is derived for MR under unidirectional loading. The frictional contact of the MR wire during deformation is expressed as different combinations of the micro-spring states. A ratio coefficient is applied to reflect the anisotropy property of MR. All the enhancements have been already applied to the micro-spring model. The feasibility of the model is verified by comparing the analytical results computed by the theoretical model, the numerical results using ADAMS dynamic simulation of a MR virtual prototyping model, and the experimental results of MR under unidirectional tests. The accuracy of the model is also compared with other constitutive models such as the porous material model and the curved cantilever beam model.

2. THE EQUIVALENT STIFFNESS OF THE MICRO-SPRING

2.1 Spatial distribution of micro-springs

The mechanical properties of MR are related to the wire material and dimension such as the diameter and the relative density. In addition, the properties in the forming pressure direction are different from those in the non-forming pressure direction [17]. A helical micro-spring with radial shear and axial elastic deformation was constructed to represent the micro-unit within the MR, as shown in Fig. 2. It can be subjected to axial load, torque, bending moment, and radial shear [18]. The axial and radial force components of the micro-spring under load along the forming direction are decomposed as

$$\begin{cases} F_z = F\sin\varphi \\ F_r = F\cos\varphi \end{cases} \tag{1}$$

where φ is the orientation angle, defined as the acute angle between the radial force F_r and the loading force F.

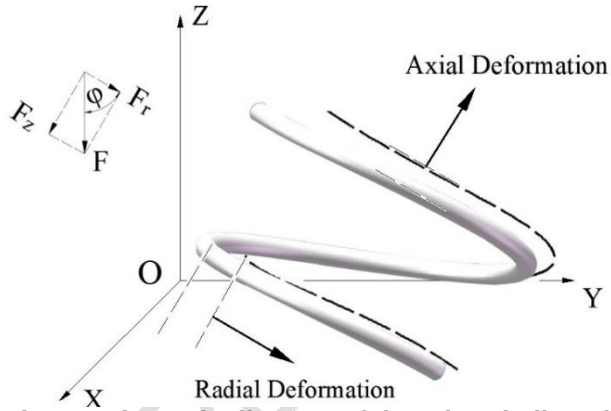

Fig. 2. Schematic diagram of the micro-helix unit

Before cold-pressed, the helical spring-units are randomly oriented with a uniform orientation angle over $[0,\pi/2]$. The subsequent forming process leads to an increase in the contacts between the coils. As a consequence, the inclination angles no longer follow a uniform distribution but tend to cluster around skewed angles. According to the Pauta criterion, assume φ has a normal distribution with a mean value of $\bar{\varphi}$ and a standard deviation of $\bar{\varphi}/3$. The probability density function of φ can be written by

$$f(\varphi) = \frac{1}{\frac{\sqrt{2\pi}}{3}\bar{\varphi}} \exp\left[-\frac{1}{2}\left(\frac{\varphi - \bar{\varphi}}{\frac{1}{3}\bar{\varphi}} \right)^2 \right] \tag{2}$$

where

$$\bar{\varphi} = \arctan\frac{1}{r} \tag{3}$$

and r is the molding rate, normally between 3 and 5 [19]. The probability density function curve with molding rate of 3 is shown in Fig. 3.

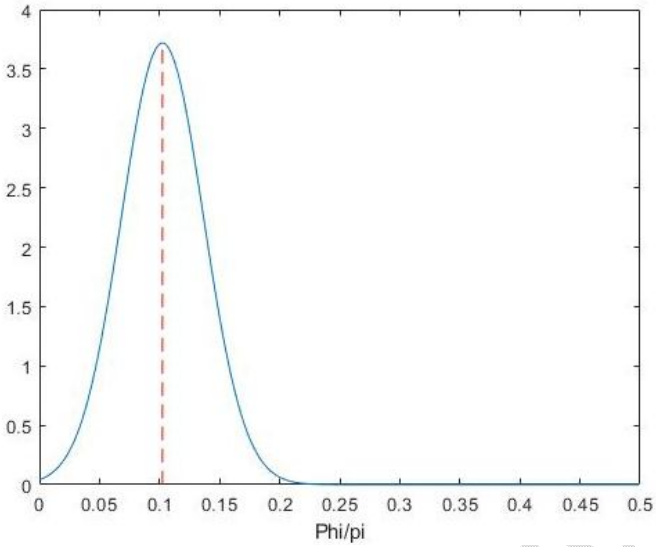

Fig. 3. Probability density function curve for normal distribution with molding rate of 3

2.2 Loading analysis of micro-springs

The deformation of the micro-spring during compression is assumed to be uniform throughout without fracture, and to maintain its helical shape. An arbitrary cross-section S in perpendicular to the axial direction of the wire is picked up in the helical spring, where the micro-unit is taken. With the central point O of the S-section as the coordinate origin, a global coordinate frame O-xyz and a reference coordinate frame O-abn are founded. Where a and b are mutually vertical radials on the S-section, the a-axis is on the horizontal xy-plane, the n-axis is perpendicular to the S-section as the axial direction of the wire, and α is the angle between the n-axis and t-axis on the xy-plane as the helix angle.

As shown in Fig. 4, the micro-unit is subjected to a force F_z along the z-axis and a moment M_t along the t-axis in the global coordinate frame xyz upon the imposition of axial loading. The F_z and M_t are decomposed into the reference coordinate frame abn to obtain the components in each direction as

$$\begin{cases} F_n = -F_z \sin\alpha \\ M_t = \dfrac{1}{2} F_z D \\ M_b = -M_t \sin\alpha \\ T_n = M_t \cos\alpha \end{cases} \tag{4}$$

where D is the diameter of the micro-spring, and d is the diameter of the wires. Generally, the influence of shearing is neglected for slender beams. The axial deformation of the micro-spring along the loading direction is expressed by the Castigliano's second theorem as

$$\Delta z = \int_0^l \frac{\partial T_n}{\partial F_z} \frac{T_n}{GI_p} ds + \int_0^l \frac{\partial M_b}{\partial F_z} \frac{M_b}{EI_b} ds + \int_0^l \frac{\partial F_n}{\partial F_z} \frac{F_n}{ES} ds \tag{5}$$

define

$$ds = \frac{D}{2\cos\alpha} d\theta \tag{6}$$

is the polar angle of the micro-unit from the xz-plane to any vertical section of the infinitesimal coil. The rigidity modulus is expressed for isotropic material as

$$G = \frac{E}{2(1+\upsilon)} \tag{7}$$

where E is the modulus of elasticity, and υ is the Poisson's ratio. The moments of inertia of the cross-section of the micro-spring including the polar moment can be indicated as

$$\begin{cases} I_a = I_b = \dfrac{1}{64\pi d^4} \\ I_p = \dfrac{1}{32\pi d^4} \end{cases} \tag{8}$$

The deformation of the micro-spring along the axial direction is obtained at $l = 2\pi$. Substituting Eqs. (4), (6) and (7) into Eq. (5) yields

$$\Delta z = \frac{4F_r D\left[4(1+\nu)D^2\cos^2\alpha + \left(4D^2 + d^2\right)\sin^2\alpha\right]}{Ed^4\cos\alpha} \tag{9}$$

and then the equivalent stiffness of the counterpart gives

$$k_z = \frac{F_z}{\Delta z} \tag{10}$$

Fig. 5 indicates that the average distance δ from the stressed section to the end is half pitch. The micro-unit is subjected to a force F_r along the y-axis, a moment M_x along the x-axis and a moment M_z along the z-axis in the global coordinate frame xyz upon the imposition of radial loading. The F_r, M_x and M_t are decomposed into the reference coordinate frame abn to derived the components in each direction:

$$\begin{cases} \delta = \dfrac{1}{2}\pi D\tan\alpha \\ M_a = M_x\sin\theta \\ M_b = -M_x\cos\theta\sin\alpha - M_z\cos\alpha \\ T_n = M_x\cos\theta\cos\alpha - M_z\sin\alpha \\ F_n = -F_r\sin\theta\cos\alpha \\ M_x = F_r\cdot\delta \\ M_z = \dfrac{1}{2}F_r D\sin\theta \end{cases} \tag{11}$$

Rigorously, a total coil of the micro-spring is the parallel connection of two perfectly symmetrical half-coils, which means that the radial deformation along the load direction is expressed by the Castigliano's second theorem while $l = \pi$ as

$$\Delta r = \frac{1}{2}\left(\int_0^l \frac{\partial T_n}{\partial F_r}\frac{T_n}{GI_p}ds + \int_0^l \frac{\partial M_a}{\partial F_r}\frac{M_a}{EI_a}ds + \int_0^l \frac{\partial M_b}{\partial F_r}\frac{M_b}{EI_b}ds + \int_0^l \frac{\partial F_n}{\partial F_r}\frac{F_n}{ES}ds\right) \tag{12}$$

Considering Eqs. (6), (7) and (11), Eq. (12) can be rewritten as

$$\Delta r = \frac{2F_r D^3\left[\nu\left(\pi^2+1\right)\sin^2\alpha + 2\pi^2\tan^2\alpha + 1\right] + Dd^2\cos^2\alpha}{Ed^4\cos\alpha} \tag{13}$$

and then the equivalent stiffness of the counterpart gives

$$k_r = \frac{F_r}{\Delta r} \tag{14}$$

Nevertheless, the complicated and disordered spatial distribution of the wires in MR reveals the fact, which the actual loading on micro-springs goes beyond individual axial or radial loads and contains combinations of them as well. Therefore, the equivalent stiffness of the micro-spring model with an arbitrary spatial angular distribution under loading along the forming direction can be defined as

$$k_{\varphi} = k_z \sin\varphi + k_r \cos\varphi \tag{15}$$

then substituting Eqs. (9), (10), (13) and (14) into Eq. (15) yields

$$k_{\varphi} = \frac{Ed^4 \cos\alpha \sin\varphi}{4D\left[4D^2(1+\nu)\cos^2\alpha + \left(4D^2 + \mathrm{d}^2\right)\sin^2\alpha\right]} + \frac{Ed^4 \cos\alpha \cos\varphi}{2D^3\left[\nu\left(\pi^2+1\right)\sin^2\alpha + 2\pi^2\tan^2\alpha + 1\right] + d^2\cos^2\alpha} \tag{16}$$

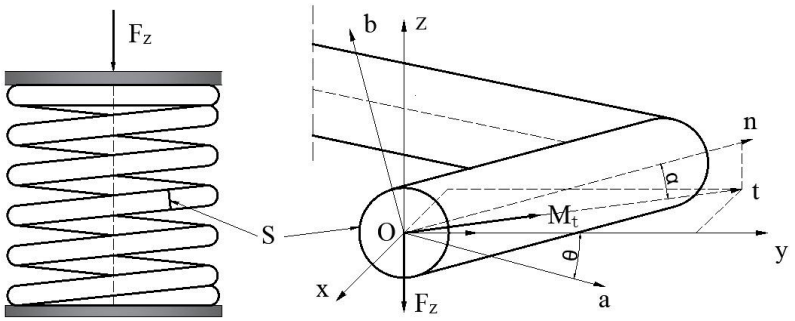

Fig. 4. Analysis of axial loading on the micro-unit

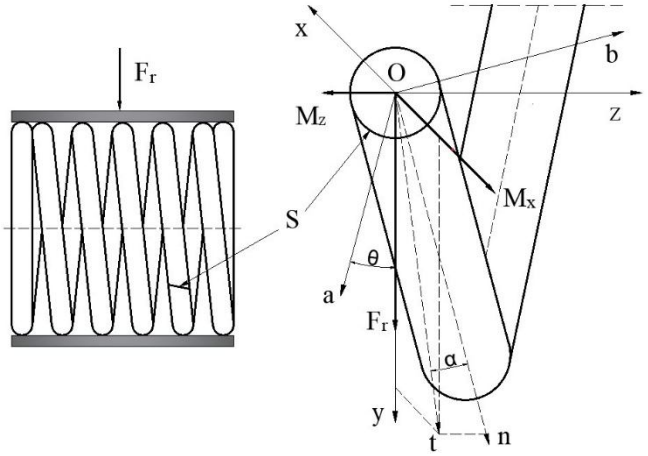

Fig. 5. Analysis of radial loading on the micro-unit

2.3 Frictional contact state of micro-springs

Notice that the disordered spatial distribution of micro-springs and the states of frictional connections between them all give contributions to the unpredictable nonlinear intrinsic behaviour of MR. The research shows that the helical coils are stacked mutually in space with non-contact, extrusion, friction and slippage, and the states within the wires provide the primary dependence for energy dissipation [20]. And those simultaneously various contact states of the internal micro-units affect the stiffness and damping properties of MR in diverse patterns, which proceed through a transition from non-contact to sliding-contact, and then viscous extrusion. Zhu [21] graphed the transformation of the percentage of the number of micro-elements in each contact states throughout the loading procedure. And Ren [22] determined the proportions of wires for non-contact, sliding-contact and viscous extrusion by reconstruction and separation of the numerical model, and the statistical classification.

As shown in Fig. 6, in this paper, the distribution for contact states of micro-springs is approximated and plotted based on the probability density curve of the normal distribution for

the spatial orientation angle in MR and dynamic changes in relative displacement due to indirect contact between turns. In the initial strain phase, the wires inside MR are constantly forced to approach themselves under the imposed loads, thus leading to a dramatic reduction in the proportion of non-contacting micro-springs and an increment in sliding-contact. And the number of sliding-contact states attains a certain value and starts to decline, while the viscous extruded micro-springs grows rapidly with the loads sustained. Then the non-contact state of the micro-springs gradually fades away while the free-space among wires proceeds to minimize, and the ratio of individual contact states tends to be comparatively steady in the final stage of adaptation.

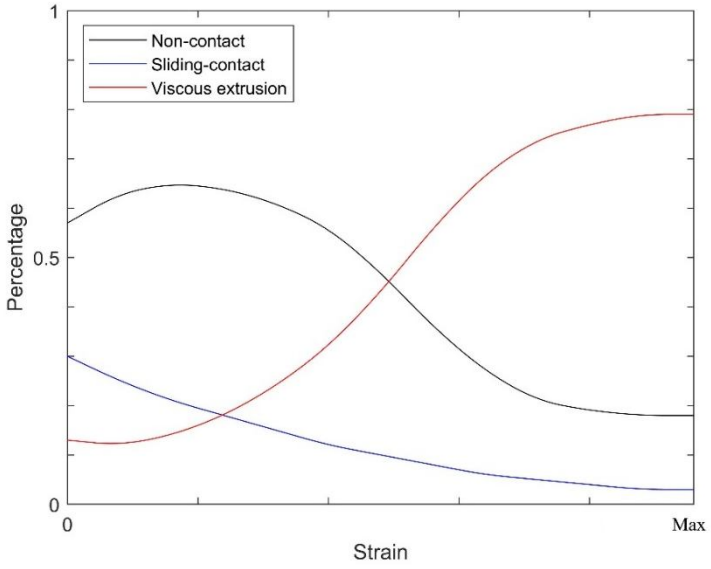

Fig. 6. Proportion of contact states distribution in MR

Therefore, the equivalent stiffness of the micro-unit is further modified by mechanical analysis of the micro-springs with different contact states, which involves the frictional coefficient of the material of the wire spiral coil. Fig. 7 shows that the lower micro-element is not exposed to any external force from the upper layer when the micro-spring in the non-contact state is loaded, due to the large clearance between the micro-springs. At this point, the deformation in the non-contact state originates merely from the elasticity of the upper portion, and the equivalent stiffness of this part is modified by

$$k_a = k_{\varphi 1} \tag{17}$$

The supporting force F_n, the sliding friction F_f, the corresponding reaction force F_n' and F_f' are generated between the micro-elements with the transition occurring, while the state of the micro-spring is slowly updated from non-contact to sliding-contact. The micro-springs originally in parallel or perpendicular states are hooked together once multiple monomers are touched mutually, presenting the initial state of nested, squeezed and stacked spiral wires. As shown in Fig. 8, the model of sliding-contact is explained for the situation in which two micro-springs exactly touch, and thus generate slippage. Based on the hysteresis constitutive model of MR by Zhu [17], the equivalent stiffness of the micro-spring is derived as

$$k_b = \frac{k_{\varphi 1} k_{\varphi 2}}{\varphi_f k_{\varphi 1} + k_{\varphi 2}} \tag{18}$$

where

$$\varphi_f = 1 + \frac{\sin|\varphi_1 - \varphi_2| - f\cos|\varphi_1 - \varphi_2|}{\cos|\varphi_1 - \varphi_2| + f\sin|\varphi_1 - \varphi_2|} \cdot \tan|\varphi_1 - \varphi_2| \tag{19}$$

and f is the sliding frictional coefficient of the material.

Furthermore, with the rise of the external loads, the squeezing of the wires limiting the slippage is observed. As shown in the viscous extrusion model of Fig. 9, the contact state of the micro-elements is viscous and approaches parallel structure, which could be characterized as the superposition of spiral wires. And the process of continuous transformation of the micro-spring into viscous extruded state is considered to be the base of the overall structural strength and stability for MR. Thus, the model stiffness which is equivalent to the sum of both stiffnesses is deemed to be

$$k_c = k_{\varphi 1} + k_{\varphi 2} \tag{20}$$

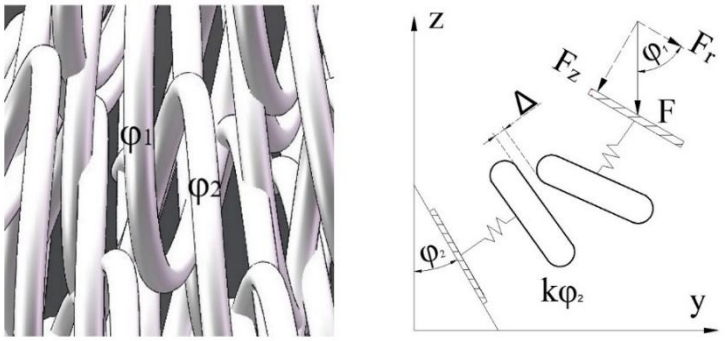

Fig. 7. Non-contact model of micro-spring

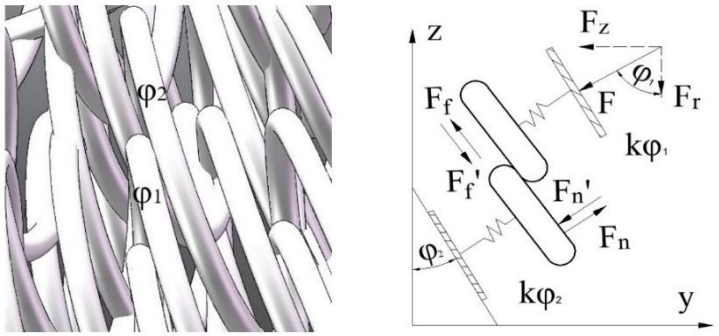

Fig. 8. Sliding-contact model of micro-spring

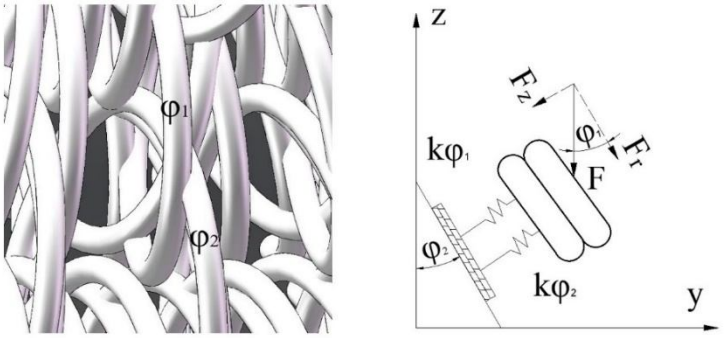

Fig. 9. Viscous extrusion model of micro-spring

The prediction of the ratio of static frictional contact and viscous extrusion within the material during compression is the essential measure for the construction of equivalent stiffness. A certain gap between each contact state grants elasticity to MR. And the gap of the wires in non-contact state tends to reduce with growing compression, while the wires in the sliding frictional state approaches to zero. Eventually, the MR turns into an approximately rigid body with minimal elasticity in case all the gaps are totally compressed.

3. CONSTITUTIVE MODEL OF MR

The spatial orientation angle φ, a major variable in the constitutive equation, which characterizes the spatial distribution pattern of microelements within the material, has been concerned. As shown in Fig. 10, so as to investigate the compressive deformation, a representative cubic unit of volume, as a continuous medium model in MR, is adopted.

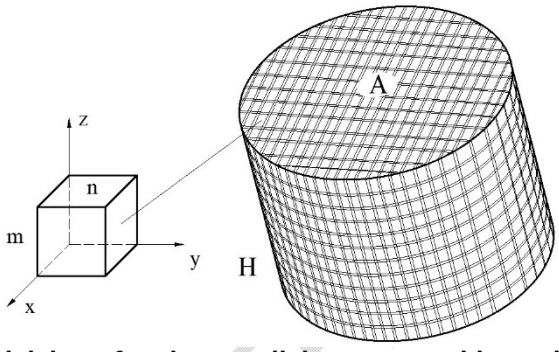

Fig. 10. Division of series-parallel structure with a cubic unit

Suppose that there are m turns in the unit length and n turns in the unit area of micro-springs. The total amount of coils within the unit of volume, deformed under the loads, is given by

$$M = \frac{4\rho_m \cos\alpha}{\pi^2 \rho_s D d^2} = \frac{4\rho \cos\alpha}{\pi^2 D d^2} \tag{21}$$

where ρ_m is the density of MR, ρ_s is the density of the wire, and ρ is the relative density (the ratio of MR density to the wire density). And assuming a uniform distribution of wire turns, the total number of layers is expressed as

$$m = M^{\frac{2}{3}} \tag{22}$$

while the amount of turns per layer gives

$$n = M^{\frac{1}{3}} \tag{23}$$

Sections of micro-springs in the upper layer are constantly and randomly embedded in the pores of the lower layer under pressure, due to the mutual sliding and squeezing of the wires. Fewer layers are deformed along the loading direction within the units, while the number of micro-springs on the unit area progressively increases, resulting in a larger relative density of MR. Suppose that the micro-springs engaged in deformation toward the loads are uniformly embedded in the layers below when MR is pressed. Thus, the amounts of layers in the unit will be also evenly reduced. And the total amount of layers can be rewritten as

$$p = m(1-\varepsilon) \tag{24}$$

while the amount of turns per layer is covered by

$$q = n + \frac{\varepsilon}{1-\varepsilon} n = \frac{n}{1-\varepsilon} \tag{25}$$

where ε is the stress for the unit of volume. The coefficients β_a, β_b and β_c are employed to represent the ratio of non-contact, sliding-contact and viscous extrusion of the micro-springs

per unit area for the loaded MR, respectively. Within the maximum range of strain, a dedicated exponential function is chosen to assume the changing stiffness of the micro-spring in a series-parallel relationship between the layers. Further, based on the equivalent stiffness expressions for the respective contact states of the micro-springs, the equal stiffness of the MR unit area is defined as

$$k_s = \left(\sum k_a \beta_a + \sum k_b \beta_b + \sum k_c \beta_c\right) \cdot a e^{b\varepsilon} \tag{26}$$

where

$$\beta_a + \beta_b + \beta_c = 1 \tag{27}$$

a and b are parameters that contribute to the complication of MR in compressed deformation under loads. Since the micro-springs of each layer are mutually parallel to the others, the equivalent stiffness of each layer is expressed as

$$k_q = \sum_{i=1}^{q} k_i = q k_s \tag{28}$$

The proportion of the micro-springs in each state varies relatively upon compressive deformation, yielding non-numerical growth for the relative stiffness., and the equivalent stiffness is modified by

$$k_{pq} = \frac{\prod_{i=1}^{p} k_{ip}}{\sum_{i=1}^{p} \prod_{j=1,\, j\neq i}^{p} k_{jq}} = \frac{q}{p} k_s \tag{29}$$

Considering Eqs. (22), (23), (24) and (25), Eq. (29) can be rewritten as

$$k_{pq} = \frac{k_s M^{\frac{1}{3}}}{(1-\varepsilon)^2} \tag{30}$$

For a MR specimen with shape factor c, the stress-strain defines

$$\frac{d\sigma}{d\varepsilon} = c k_{pq} \tag{31}$$

where

$$c = \frac{L}{A} \tag{32}$$

L is the height of the specimen and A is the cross-sectional area perpendicular to the loading direction of MR. Then substituting Eqs. (30) and (32) into Eq. (31) yields

$$\sigma = \frac{L M^{\frac{1}{3}} k_s}{A} \frac{\varepsilon}{(1-\varepsilon)^2} \tag{33}$$

A Taylor expansion of Eq. (33), taking the second-order approximation, gives

$$\frac{\varepsilon}{(1-\varepsilon)^2} = \varepsilon + 2\varepsilon^2 + 3\varepsilon^3 + o(\varepsilon^3) \tag{34}$$

By substituting Eqs. (21) and (34) into Eq. (33), and modifying the coefficients, the eventual stress-strain relationship for MR is optimized for

$$\sigma = \frac{L}{A}\left(\frac{4\rho\cos\alpha}{\pi^2 D d^2}\right)^{\frac{1}{3}} \left(\sum k_a \beta_a + \sum k_b \beta_b + \sum k_c \beta_c\right) \cdot \left(\varepsilon + 2\varepsilon^2 + 3\varepsilon^3\right) A_1 e^{B_1 \varepsilon} \tag{35}$$

where A_1 and B_1 are the updated proportional variables.

The constitutive model of micro-spring is established with unidirectional loads by Eq. (35), reflecting the impacts of parameters such as material, relative density, the diameter of wire,

the rate of molding, and the shape factor of specimen on performance for MR. Separating Eq. (35) yields

$$\begin{cases} \sigma = K \cdot \Phi \\ K = \dfrac{L}{A}\left(\dfrac{4\rho\cos\alpha}{\pi^2 D d^2}\right)^{\frac{1}{3}}\left(\sum k_a\beta_a + \sum k_b\beta_b + \sum k_c\beta_c\right) \\ \Phi = A_1 e^{B_1\varepsilon}\left(\varepsilon + 2\varepsilon^2 + 3\varepsilon^3\right) \end{cases} \tag{36}$$

where K characterizes the physical factors of the microstructure and molding parameters for MR, and Φ describes the shape of the constitutive structural curve of the model.

4. MODEL SIMULATION AND FEASIBILITY OF A METAL RUBBER SPECIMEN

4.1 The creation of virtual prototyping model

The dynamical simulation is based on a cylindrical MR specimen, with the diameter of 30 mm, height of 31.5 mm, diameter of wires 0.12 mm, diameter of spirals 1.2 mm, relative density of 0.24, molding pressure of 23 kN, material of 304 stainless steel (0Cr18Ni9), density of 7930 kg/m3, and modulus of elasticity 193 Gpa, was shown in Fig. 1 (a). The simplified model, referring to the preparation process and setting the same shape and dimensions of MR, was modelled in SOLIDWORKS to reduce the calculated volume of the numerical simulation. The constructed model, was shown in Fig. 1 (b), was imported into ADAMS (a virtual prototype) with Poisson's ratio 0.33, the modulus of elasticity and the density of the wires setting.

In the design of dynamical simulation, flexible contact, where the contact force calculated by penalizing the parameters with regression coefficients, was employed between the wires and the sliding friction coefficient was set to 0.09. Generally, the compression rate of MR is less than 30% under loading. The loading speed for the compression simulation of the MR dynamical model, considering the weaker ability to support external loads at a small relative density, was fixed to 1 mm/min. In addition, the loading method was uniaxial and unidirectional while the loading surface was the molding surface of the MR model, thus the whole loading process was considered as a static process due to the slow loading rate. A half period of force in static compression was showed in Fig. 11.

The axial stiffness of MR was nonlinear and accompanied by a turbulent upward tendency, while the compression gradually increased from the whole viewpoint. In the structural aspect, the phenomenon, with unstable growth in stiffness, is explained that the gradual increasing of the relative density in the loading process for MR leads to progressive increases in the number of spirals inside the unit, and the capability of each unit improves to withstand the payload. The whole changing process in stiffness are roughly divided into a short linear elastic phase at initial loads, a soft feature phase with large variations during loading, and a stable hardening phase in the later stages.

In the linear elastic phase, most of the non-contacting micro-springs start to slide mutually due to the external forces, and the reason behind the almost invariable stiffness of MR is the continuous embedding of the wires in the structural gaps. In the soft feature phase, the mainly contact state transition occurs from the slippage to the viscous extrusion, which is associated with a more pronounced change in the stiffness of the MR. Along with the growth of loads, the relative compression of MR progressively gets smaller, which causes the wires to give viscous characteristics. In the stable hardening phase, the gaps inside the MR become narrower and narrower, and the vast majority of the wires, making the whole structure more stabilized, are in the viscous extrusion state. The stiffness of MR is also large

and changes rapidly with the fact, in which the relative density reaches a high value and tends to be fixed. The mechanical properties of MR with high-relative density are significantly reduced when the subjected loads enlarge to a certain level, which was also reported by Zhang [23]. Further, MR is squeezed to a rigid body similar to an inelastic body once the magnitude of the loads exceeds a threshold value to withstand.

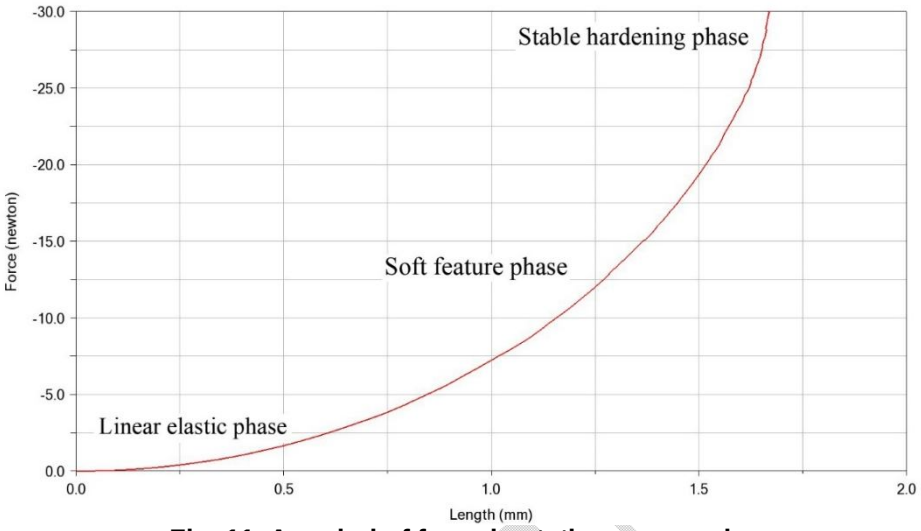

Fig. 11. A period of force in static compression

4.2 The creation of virtual prototyping model

The energy conversion of MR is divided into storage of deformation energy, which relies on the elastic work of the external force to the equivalent unit, and dissipation of internal energy, which determined by the partial mechanical energy generated by the contact sliding friction between the equivalent units. Therefore, the hysteresis characteristic borrowed from the macroscopic stress-strain curve of MR under the cyclical loading condition, is presented.

In the practical experiment, the MR specimen, shown in Fig. 1 (a), with a loading frequency of 2 Hz (which can be approximated as static loading) and an amplitude of 1 mm, was used for sinusoidal loading on a servohydraulic material testing machine at room temperature. To minimize the uncertainty of this measurement, a preload of 1.5 mm was applied to weaken the effect of the non-complete contact surface. The same tests have been simulated on the virtual prototype. The stress-strain hysteresis curve of the material, with processing the data according to the shape and size of the metal-rubber specimen, was obtained. By substituting the known process parameters into Eq. (36) and combining the experimental data, the constitutive equation of loading-unloading along the molding direction could be obtained. Fig. 12 shows a comparison of the analytical results computed by the theoretical model, the numerical results using ADAMS dynamic simulation of the virtual prototyping model and the experimental results of MR specimen under unidirectional tests.

To validate the feasibility of the model, residual analysis is used to process the data. And residual analysis is an effective means of assessing the accuracy of the model through the difference between the actual value y_i and the predicted value $\hat{y}_i$. Normally, the coefficient of determination R^2 is measured by the change of data to characterize the effectiveness of a model, which expressed as

$$R^2 = 1 - \frac{\sum_{i=1}^{n}(y_i - \hat{y}_i)^2}{\sum_{i=1}^{n}(y_i - \bar{y})^2} \tag{37}$$

where n is the number of samples and $\bar{y}$ is the mean of the observed value. The closer the value of R^2 to 1, the better the variables of the equation explain the model, while the closer to 0, the worse the model fits.

The residual analysis of the three values for each model as showed in Table. 1. The value of R^2 for the MR specimen revealed that the theoretical results of the specimens in the loading and unloading stages coincided well with the dynamical simulation results and experimental results, which verified the feasibility of the enhanced micro-spring model. Thus, the mechanical properties of MR would be predicted by the model at a certain extent. Also, the results demonstrated the feasibility of MR dynamical simulation in the virtual prototype.

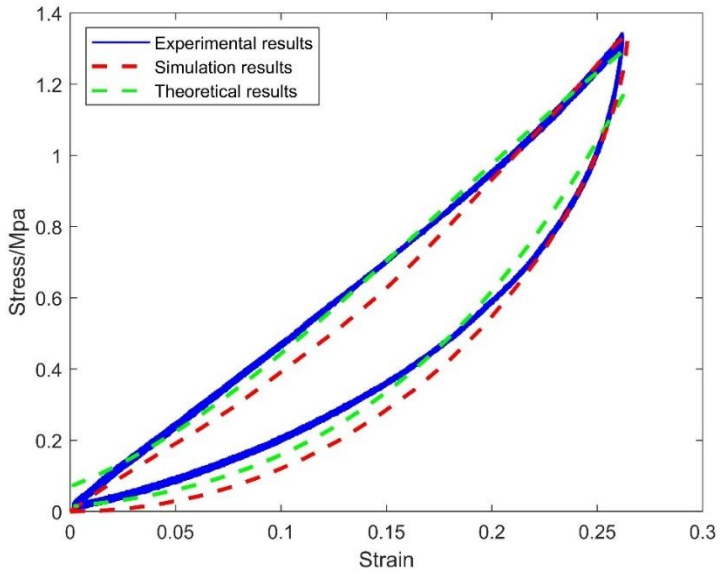

Fig. 12. The stress-strain curve of theoretical model, dynamic simulation model and practical experiments

Table 1. Residual analysis for the MR specimen

Coefficient of determination	Theoretical values towards dynamical simulation values	Theoretical values towards experimental values
R^2	0.9873	0.9839

5. COMPARISON OF CLASSICAL MODELS

Metal rubber, since its invention in 1960s, being a structural damping material with excellent load-bearing capacity and resistance to low temperature, has been repeatedly studied and tested for its static and dynamic mechanical properties through a combination of theory and experiment. In this part, the accuracy of the model proposed is verified by comparing the porous model and the curved cantilever beam model.

5.1 Porous material model

The cubic micro-unit is employed in porous theory due to the presence of MR, as a porous material with an elastic mesh structure. Assuming that the micro-unit is a hollow cube, which conforms to the continuous medium model, as shown in Fig. 13 (a). The axial deformation of the porous wall is not involved instead the bending displacement of the material when the loads applied. The relative density of the MR is denoted by the porosity, and the relations between the elastic modulus of the material, the yield stress and the density of MR are investigated. The primary equation for porous material loaded by compression was established as [9,19]

$$\begin{cases} F = A_1\left(\dfrac{E_s S\bar{\rho}^2}{72H}\right)X + B_1\left(\dfrac{E_s S\bar{\rho}^2}{72H^2}\right)X^2 + C_1\left(\dfrac{E_s S\bar{\rho}^2}{72H^3}\right)X^3 \\ E_s = \dfrac{3EhD^4}{8d^5} \end{cases} \tag{38}$$

where E_s is the modulus of elasticity for the porous material, S is the loaded cross-sectional area, H is the initial height of the specimen, $\bar{\rho}$ is the initial relative density of the MR, h is the pitch, A_1, B_1 and C_1 are the fitting coefficients.

5.2 Curved cantilever beam model

From the fine point of view, MR, at a particular angle with the molding direction, can be regarded as consisting of numerous curved cantilever beams. The elastic deformation between the curved beams and the slip between the wires determines the mechanical performance of the loading MR. A fine-scale MR model with a single-turn spiral coil composed of multiple parallel curved cantilever beams as the basic unit shown in Fig. 13 (b), which explained the mechanism of deformation and the essential characteristics of nonlinearity, was constructed. The relationship of stress-strain for the cantilever curved beam model is followed as [10]

$$\sigma = A_1 E\left[\left(\frac{d}{D}\right)^{10}\rho\right]^{1/3}\left(1-B_1\varepsilon\right)^{-3}\varepsilon \tag{39}$$

where A_1 and B_1 are the fitting coefficients.

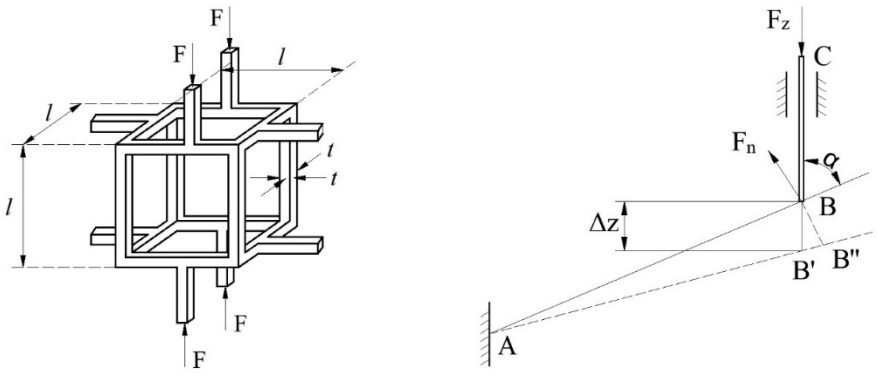

(a) Porous material model (b) Curved cantilever beam model

Fig. 13. Classical mechanical models of MR

5.3 Comparative analysis results of the models

Both the porous material model and the cantilevered curved beam model, which explained the special mechanical properties from the appropriate perspectives based on the structure of MR, have modelled the mechanics, yet there are still controversies with the real structure.

In details, the modelling error of the porous model is quite obvious due to the adoption of hollow cubes to denote the irregular structural gaps of MR, while the embedding of the curved beam in compression is not addressed in the modelling process for the curved cantilever beam model.

The MRs, relative densities of 0.2 and 0.25, was simulated in ADAMS. The accuracy of the three constitutive models for MR, by fitting the data, was compared, and the results are shown in Fig. 13 and Fig. 14. The results concluded that the values, which predicted by the constitutive models of MR, exhibit limitations in fitting the simulated data. Furthermore, experimental residual analysis of the adapted strain values for each model was performed to evaluate their accuracy in loading-unloading tests on MR as showed in Table. 2.

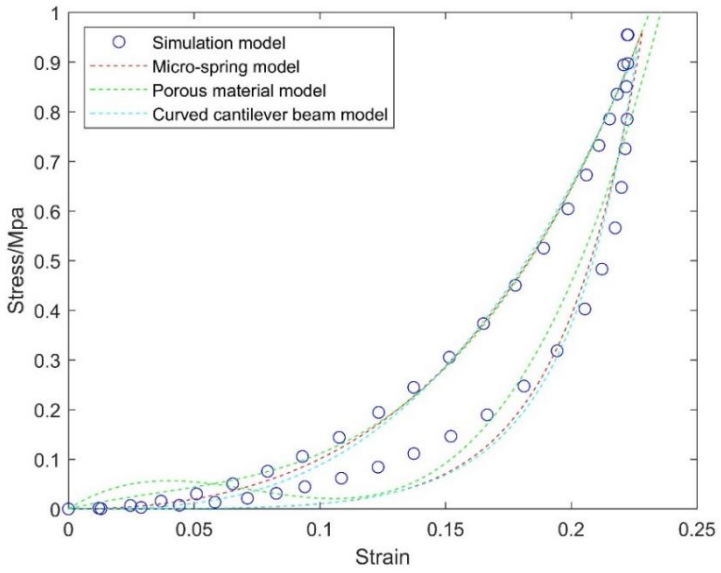

Fig. 14. Classical mechanical models of MR

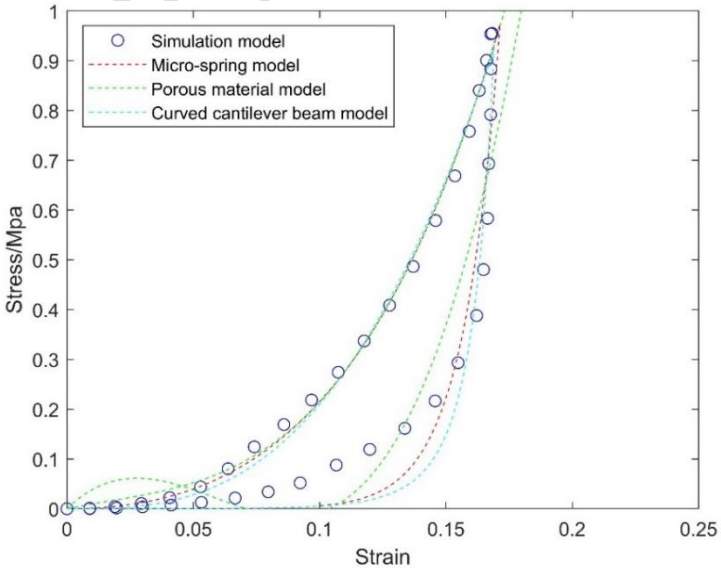

Fig. 15. Classical mechanical models of MR

Table 2. Residual analysis for the classical models

Coefficient of determination	Relative density of MR	Curved cantilever beam model	Porous material model	Enhanced micro-spring model
R^2	0.2	0.9587	0.9368	0.9595
	0.25	0.9387	0.8710	0.9530

The comparison results indicated that the average error of the simulation data for the proposed model, being compared with the classical porous material model and cantilever beam mechanics model, was relatively smaller. Therefore, the stress-strain correlation between MR and its structural parameters such as the material of wire, the diameter of wire, the diameter of spiral coil, relative density, and external dimensions, under static pressure, is better characterized by this mechanical model in a more comprehensive and accurate way. The association among the complicated micro-contact friction between metal wires and the nonlinear mechanical behaviour could also be effectively explained by the model.

6. CONCLUSION

In this study, an enhanced micro-spring model that employs adaptively deformed micro-springs with random spatial distribution, which involves the micro-contact frictional states and contains macroscopic and microstructural parameters, has been adopted to MR. To generalize, the characteristics of MR are well modelled in this model and the following main conclusions can be derived:

(a) The theory of static compression and the phenomenon of complicated micro-contact friction for MR are explained by the variation of equivalent stiffness;
(b) The feasibility of the model is verified more convincingly by theoretical model, dynamic simulation model and practical experiments in combination;
(c) The error produced by fitting the proposed model to the data is smaller and acceptable in comparison with the porous material model and the curved cantilever beam model.

REFERENCES

1. Д.Е. Чегодаев, О.П. Мулюкин, Е.В. Колтыгин, The Design of Metal Rubber Component, Z. Y. Li, translated in Chinese, ISBN: 9787118021813, National Defence Industry Press, Beijing, 2000.
2. D. Y. Zhang, Y. Xia, Q. C. Zhang, et al, Researches on metal rubber mechanics properties in retrospect and prospect, J. Aerospace Power. 33 (06) (2018): 1432-1445.
3. G. He, P. Liu, Q. Tan, Porous titanium materials with entangled wire structure for load-bearing biomedical applications, J. Mech. Behav. Biomed. Mater. 5 (1) (2012) 16–31.
4. X. Xue, P. Yang, Y. Shao, et al, Manufacture technology and anisotropic behaviour of elastic-porous metal rubber, J. Lightweight Materials and Manufacture. 3 (2) (2020): 88-99.
5. K. Wu, H. Bai, X. Xue, et al, Energy Dissipation Characteristics and Dynamic Modeling of the Coated Damping Structure for Metal Rubber of Bellows. Metals. 8 (7) (2018).
6. B. Zhang, Z. Q. Lang, S. A. Billings, et al, System identification methods for metal rubber devices, Mech. Syst. Sig. Proc. 39 (1) (2013): 207-226.

7. Ma, Q. Zhang, D. Zhang, et al, The mechanics of shape memory alloy metal rubber, Acta Mater. 96 (2015) 89–100.
8. P. Yang, H. Bai, X. Xue, et al, Vibration reliability characterization and damping capability of annular periodic metal rubber in the non-molding direction, Mech. Syst. Sig. Proc. 132 (2019): 622-639.
9. X. Q. Chen, B. T. Guo, Z. G. Zhu, The inestigation of the stiffness characteristics and the stress-strain relation of metal rubber, J. Aerospace Power. 17 (4) (2002): 416-420.
10. Y. Y. Li, X. Q. Huang, Static Characteristics for Metal Rubber Structure with Different Shape Factor, J. Applied Mechanics. 26 (01) (2009): 82-86+213.
11. F. L. Cao, H. B. Bai, G. Q. Ren, et al, Constitutive Model of Metal Rubber Material Based on Curved Cantilever Beam of Variable Length, Mech. Syst. Sig. Proc. 48 (24) (2012): 61-66.
12. W. J. Hou, X. Yuan, W. Yang, et al, Constitutive Model for Simply Supported Beams of Metal Rubber, Aero. Eng. 40 (08) (2021): 1299-1304.
13. D. Rodney, B. Gadot, O. R. Martinez, et al, Rodney reversible dilatancy in entangled single-wire materials, Nat. Mater. 15 (1) (2016): 72–77.
14. Y. H. Ma, D. Gao, D. Y. Zhang, et al, Compressive and dissipative behavior of metal rubber under constraints. Phys. Status. Solidi. B. 252 (7) (2015): 1675–1681.
15. K. Chandrasekhar, J. Rongong, E. Cross, Mechanical behavior of tangled metal wire devices, Mech. Syst. Sig. Proc. 118 (2019) 13–29.
16. P. Yang, H. B. Bai, X. Xin, et al, Vibration reliability characterization and damping capability of annular periodic metal rubber in the non-molding direction. Mech. Syst. Sig. Proc. 132 (2019b): 622–639.
17. J. Hong, B. Liu, D. Zhang, et al, Shape Memory Effect and Hysteresis Behavior of Shape Memory Alloy Metal Rubber, Proc. ASME Turbo Expo. 7 (2012).
18. W. Peng, H. B. Bai, J. Zheng, et al, A Micromechanics Constitutive Model of the Metal Rubber Materials Based on the Radial and Axial Combined Deformation of the Microsprings, J. Exp. Mech. (03) (2005): 455-462.
19. X. Xue, S. Ruan, H. Bai, et al. An enhanced constitutive model for the nonlinear mechanical behavior of the elastic-porous metal rubber, Mech. Mater. 148 (2020): 103447.
20. D. Zhang, F. Scarpa, Y. Ma, et al, Dynamic mechanical behavior of nickel-based superalloy metal rubber. Mater. Design. (1980-2015) (2014), 56: 69-77.
21. B. Zhu, Y. H. Ma, J. Hong, Theoretical analysis on stiffness and damping characteristics of metal rubber, J. Beijing University of Aeronautics and Astronautics. 37 (10) (2011): 1298-1302.
22. Z. Y. Ren, L. L. Shen, H. B. Bai, et al. Constitutive model of disordered grid interpenetrating structure of flexible microporous metal rubber, Mech. Syst. Sig. Proc. 154 (2021): 107567.
23. D. Y. Zhang, F. Scarpa, Ma, Y.H, et al, Compression mechanics of nickel-based superalloy metal rubber, Mater. Sci. Eng. 580 (2013), 305–312.